



UNIVERSITY OF LEEDS

This is a repository copy of *Doxorubicin-functionalized graphene nanoribbons as novel assistant for ionic liquid-based electrolyte in DSSCs: an experimental and DFT study*.

White Rose Research Online URL for this paper:

<https://eprints.whiterose.ac.uk/224189/>

Version: Accepted Version

Article:

Davoudabdollah, M., Kowsari, E., Boghrabad, M.M. et al. (3 more authors) (2025) Doxorubicin-functionalized graphene nanoribbons as novel assistant for ionic liquid-based electrolyte in DSSCs: an experimental and DFT study. *Research on Chemical Intermediates*. ISSN 0922-6168

<https://doi.org/10.1007/s11164-025-05539-y>

This is an author produced version of an article published in *Research on Chemical Intermediates*, made available under the terms of the Creative Commons Attribution License (CC-BY), which permits unrestricted use, distribution and reproduction in any medium, provided the original work is properly cited.

Reuse

This article is distributed under the terms of the Creative Commons Attribution (CC BY) licence. This licence allows you to distribute, remix, tweak, and build upon the work, even commercially, as long as you credit the authors for the original work. More information and the full terms of the licence here:

<https://creativecommons.org/licenses/>

Takedown

If you consider content in White Rose Research Online to be in breach of UK law, please notify us by emailing eprints@whiterose.ac.uk including the URL of the record and the reason for the withdrawal request.



eprints@whiterose.ac.uk
<https://eprints.whiterose.ac.uk/>

Doxorubicin-functionalized graphene nanoribbons as novel assistant for ionic liquid-based electrolyte in DSSCs: An experimental and DFT study

Mehrnaz Davoudabdollah^a, Elaheh Kowsari^{a,*}, Mohammad Mohammadizadeh Boghrabad^a, Saeedeh Sarabadani Tafreshi^a, Mahboobeh Rafieepoor Chirani^a, Nora H. de Leeuw^{b,c}

^a Department of Chemistry, Amirkabir University of Technology, No. 424, Hafez Avenue, 1591634311, Tehran, Iran

^bSchool of Chemistry, University of Leeds, LT2 9JT Leeds, UK

^cDepartment of Earth Sciences, Utrecht University, 3584 CB Utrecht, The Netherlands

Authors Emails: meda@aut.ac.ir (M. Davoudabdollah), M. Mohammadizadeh Boghrabad (mohammadmohammad@aut.ac.ir), S. Sarabadani Tafreshi (s.s.tafreshi@aut.ac.ir), M. Rafieepoor Chirani (m.chirani@aut.ac.ir), Nora H. de Leeuw (n.h.deleeuw@leeds.ac.uk)

Abstract

Dye-sensitized solar cells (DSSCs) have attracted attention due to their efficiency, and researchers are exploring various techniques to enhance their performance. Graphene nanoribbons and doxorubicin with their specific structures can improve these cells' performances. This study is the first application of doxorubicin-functionalized graphene nanoribbons (DF-GNR) as an electrolyte additive in DSSCs. One of the most innovative parts of this research is applying doxorubicin as an expired medicinal drug to embrace the circular economy. The graphene-oxide nanoribbon (GONR) synthesis began with carbon nanotube oxidation, followed by GONR and doxorubicin reacting in 1-butyl 3-methyl-imidazolium bromide (as a solvent and catalyst) and triphenyl phosphate to generate DF-GNR. The electrolytes were composed of various amounts of DF-GNR and ionic liquids, including 1-butyl-3-methyl imidazolium iodide (BMII) and 1-ethyl-3-methyl imidazolium iodide (EMII). The results showed that adding an optimum amount of DF-GNR increased the open-circuit voltage (V_{OC}) from 0.713 to 0.749 V, the short-circuit current

* Corresponding author.

E-mail address: Kowsarie@aut.ac.ir (E. Kowsari)

density (J_{SC}) from 8.559 to 13.781 (mA/cm²), and the DSSCs' efficiency from 4.276% (the standard cells based on a graphene-free electrolyte in which DF-GNR is not added.) to 7.126%. Furthermore, Density functional theory studies revealed that the adsorption of DF-GNR electrolyte additives onto the TiO₂ surface induced the formation of mid-gap states within the electrode's bandgap. These states facilitated electron transport by lowering the energy barrier, leading to a reduction in the bandgap caused by additive adsorption. This change also resulted in a redshift in the absorption edge and a significant enhancement in the efficiency of DSSCs.

Keywords: Dye-sensitized solar cell, Doxorubicin, Ionic liquid, Density functional Theory, Functionalized Graphene nanoribbon, Nano-composite electrolyte

1. Introduction

The DSSC, a favorable and reliable photo-electrochemical device to convert solar power into electrical power, has generated considerable interest on account of its low costs of production, comparatively high efficiency of energy conversion, excellent nontoxicity, and lighter weight in comparison to traditional silicon-based cells.[1–9] DSSCs consist of a transparent conducting substrate (TCO), a mesoporous, a counter electrode, nanostructured semiconductor (photo-anode), dye molecules (sensitizer), and an electrolyte.[10–14] The electrolyte plays a leading role in DSSCs due to the fact that its properties significantly impact the performance of DSSCs, which includes their conversion efficiency and stability, by regulating the dynamics of electron transfers that control the kinetics of dye regeneration.[15,16] For DSSC applications, numerous types of electrolytes, including liquid electrolytes with organic solvents, polymer gel electrolytes, inorganic materials, ionic liquids, and organic hole-transport substances, have been established.[17] Due to their superior performance in converting energy compared to other types of electrolytes, liquid electrolytes frequently serve as a medium of transportation for DSSCs. DSSCs with liquid electrolytes have seen photo-energy conversion efficiencies (PCEs) as high as 12% thus far.[18] In DSSC, charge transport and dye regeneration between the electrodes and electrolytes are both accomplished by the redox couple (I^-/I_3^-), a crucial electrolyte component, owing to its unique characteristics, high conductivity, and good solubility in solvents. This redox system has received the most attention for DSSCs in their development.[19] Organic solvent-based electrolytes, due to their low viscosity, high efficiency, ease of design process, and rapid ion diffusion, have been frequently utilized

in DSSCs. Nonetheless, one of the primary issues with the use of an organic solvent electrolyte is its low long-term stability, which is a result of its low boiling point, high temperature instability, leakage, easy evaporation, and sealing difficulty.[20] Ionic liquids (ILs) consisting of anion and cation are particularly favorable materials that could replace organic solvents in electrochemical devices because of their non-volatility, low ionic conductivity at room temperature, and great chemical and thermal stability. Utilizing the ILs-based electrolytes can address the issue of liquid electrolyte's leakage. But solvent exclusion in the electrolyte can easily result in serious issues such as decreased cell performance, potential dye detachment, and solvent volatilization, which restrict the commercial viability of DSSCs. [21,22] Substituting liquid electrolytes with nanocomposite electrolytes is an effective and straightforward method for enhancing the DSSCs' stability and photovoltaic performance. Carbonaceous materials are recognized as impressive nanofillers (NFs) for electrolytes of DSSC due to their exceptional structural, mechanical, and electrochemical adaptability. The best options for carbonaceous nanomaterials as additives in ILs-based electrolytes are carbon nanotubes, graphene derivatives, and carbon black. Electrolytes with carbonaceous nanomaterials create continuous ion-conduction pathways. These NFs' electrical conductivity is reliant on the characteristics of the electrolyte components and the properties of the carbonaceous nanomaterials, which are related to conductance, such as the porosity, shape, particle size, and functional groups on the materials' surfaces. To improve biocompatibility and solubility, the carbon nanomaterials' surfaces are capable of being changed using carbon structures with oxygen-containing functional groups.[23–29] Graphene nanoribbons (GNRs) have drastically different qualities than other forms of carbon. GNRs as thin, elongated graphene strips with a finite width (straight and high length-to-width ratio edges) have also been the topic of intense investigation. Due to their large surface area and exceptional electronic properties, GNRs are ideal fillers for nanocomposite materials.[30–32] Graphene nanoribbons of different widths can be produced, according to recent experiments employing epitaxial growth and the mechanical method.[33] Additionally, extensive research has been conducted on two top-down synthesis techniques for the production of GNRs. Graphene or graphite precursors are cut or etched into thin strips in the first method, while carbon nanotubes (CNTs) are longitudinally unzipped in the second method[34–36]. Their electronic properties are significantly influenced by the atomic structure of their edge topologies. The graphene's existence of edges significantly affects the spectra of π electrons with low energy. The qualities of graphene nanoribbons are determined by two fundamental edge shapes: armchair and zigzag.[33] Nakada et al. came to the conclusion that 3 or 4 zigzag sites per sequence are efficient for one edge state to be noticed in GNR using tight-binding band calculations.[37] According to Fujita et al.

and Son et al., as GNR's width increases, the normalized density of states decreases significantly [38,39]. This indicates that GNR has a greater electronic structure than graphene, which makes it a desirable nanofiller for electrical applications. Few experiments have yet emphasized the electrical properties of GNR nanocomposites.[40]

Waste materials containing nitrogen have recently been studied as components for graphene-based composites used in DSSCs. An eco-friendly, easy, and affordable process for efficiently converting industrial waste lignin—a byproduct of black liquor used to make paper—into oxygen-nitrogen-sulfur codoped porous carbon has been developed in that study using preoxidation and self-activation. Following self-activation, the preoxidation process strengthened the crosslinking between lignin molecules, resulting in a more disordered carbon structure and finally improving the conductivity and cells' efficiency. [41]

Doxorubicin, commonly referred to as Adriamycin, is an antibiotic classified within the anthracyclines group. [42] Doxorubicin molecules have structures that promote efficient electron transport and improve electrical conductivity. This research utilized expired doxorubicin, aiming to promote the growth of the circular economy and enhance the DSSCs' efficiency owing to the unique molecular structure of doxorubicin. In the effort to ensure drug accessibility for the public, there is a possibility that significant quantities of pharmaceuticals expire and become waste. Pharmaceuticals are disposed of using a variety of techniques, including waste encapsulation and chemical decomposition. Nonetheless, these procedures provoke apprehensions as they result in the discharge of pharmaceuticals and possibly hazardous compounds into the environment. [43,44] An opportunity exists to convert expired medications into functional materials, so minimizing waste and fostering sustainable development. Using expired pharmaceuticals in photovoltaic cells can be a new research area centered on pharmaceutical waste management. The results demonstrate a viable and efficient method for recycling expired pharmaceuticals by using the intrinsic properties of doxorubicin and the synergistic effects of the resultant compounds to produce high-performance DSSCs.

In this study, an intriguing and innovative method for improving the efficiency of DSSCs via synthesizing DF-GNR and utilizing it as an efficient additive is examined. Doxorubicin enhances the properties of GNR and can transform it into a distinctive and fascinating compound. In addition, the pollution caused by medicine disposal can be considerably reduced through using expired Dox. In BMII and EMII ionic liquid-based electrolytes, GNR leads to speeding up the exchange and ion transport. Meanwhile, the presence of Dox as a nitrogenous substance in their

structure accelerates these processes. The computational and experimental results of this work have revealed the significant effects of Dox on GNR.

2. Experimental

2.1. Materials and chemicals

Merck (Darmstadt, Germany) provided some chemicals such as carbon nanotube powder (purity > 99.99%), iodine (I₂, purity > 99.99%), lithium iodide (LiI, purity = 99.9%), potassium permanganate (KMnO₄, purity > 97.5%), ethanol (purity > 99%), ammonia (NH₄OH, purity > 99.95%), sulfuric acid (H₂SO₄, purity > 99.99%), 1-methylimidazole (purity = 99%), and hydrochloric acid (HCl, purity = 36%) except butyl iodide (purity = 99%), Triphenyl phosphate (TPP, purity > 99%), N, N-di-methyl-acetamide (purity > 99%) and methyl iodide (purity > 99%) purchased from Sigma Aldrich (Milwaukee, WI) and 4-tert-butylpyridine (TBP, purity = 99%) obtained from Exir GmbH (Wien, Austria). Also, expired doxorubicin drug (C₂₇H₂₉NO₁₁) with purity of 99% manufactured by TTY Biopharm, was provided. The rest of the solvents and materials were ordinary commercial items of analytical quality with no more purification.

2.2. Synthesis of ILs

The papers describe how to produce EMII and BMII. [21,45,46] The synthesis of BMII involves the following steps: A molar ratio of 1:1 of methyl imidazole and butyl iodide is mixed in a reflux condenser-equipped three-neck flask with a round bottom and an inlet of Ar, and fitted with a magnetic heat stirrer. Initially, 1-methylimidazole, having a higher boiling point, is introduced into the balloon, followed by the slow, dropwise addition of butyl iodide. The mixture of reaction was stirred gradually over a period of 48 hours at room temperature.

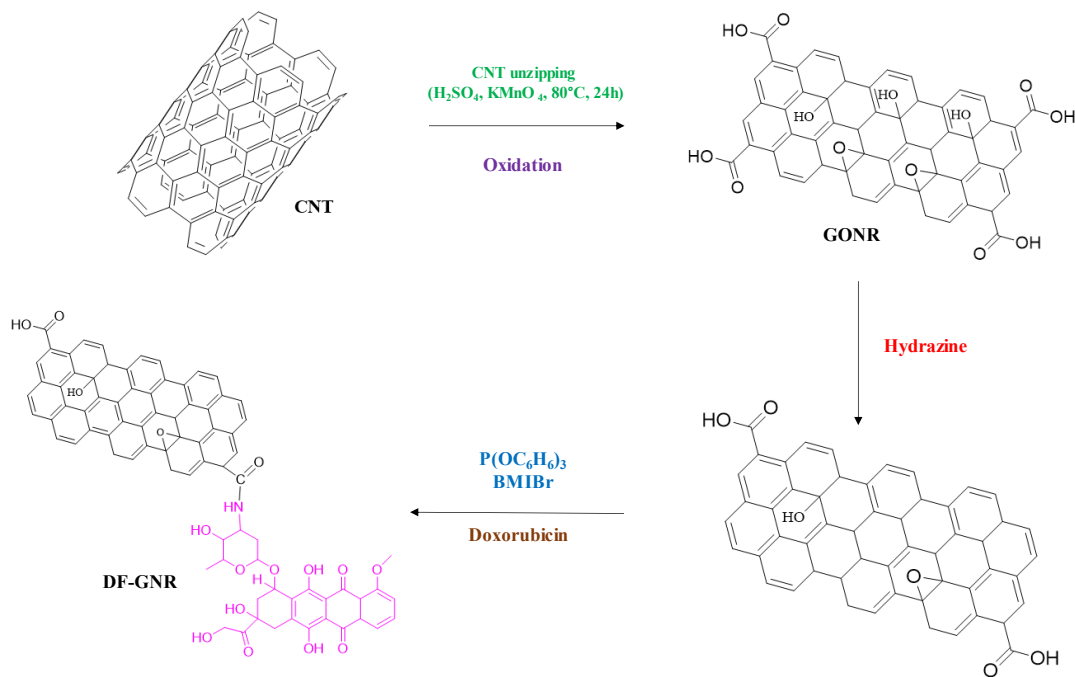
The reaction leads to the creation of a viscous liquid with a distinct orange color, which undergoes purification through multiple processes. The orange substance was obtained through two washings with ethyl acetate (an ionic liquid that is insoluble in ethyl acetate, while methyl imidazole and butyl iodide are soluble in it). This method effectively separates the impurities from the starting materials. Subsequently, the compound was dried in a vacuum oven at 35 degrees Celsius for five hours.

The synthesis of EMII follows the same procedure, conditions, and ratios as the synthesis of BMII.

2.3. Synthesis of GONR and DF-GNR:

The synthesis of GONR and DF-GNR is shown in Schematic 1. The GONR was synthesized by opening the CNT using a chemical oxidation method. Due to the interaction of sulfuric acid on the CNT layers, the nanotubes were opened longitudinally, and GONR with oxygen-rich functional groups such as ketone, hydroxyl and carboxylic acid were formed. A reductant, hydrazine, was employed to reduce the GONR-containing solution. Hydrazine reduces the number of functional groups such as epoxy, hydroxyl, and carboxylic acid present on oxidized graphene nanoribbons. This reduction facilitates resonance in their aromatic rings and enhances the electrical conductivity of the graphene nanoribbons. Ultimately, this process leads to an increase in the electrolytic conductivity of the final electrolyte additive material.

The steps are as follows: Potassium permanganate (0.5 g) and sulfuric acid (100 ml) were used to disperse CNT (0.1 g). For 15 hours, the mixture was vigorously stirred with a magnetic stirrer at a temperature of 35°C. To eliminate any unreacted potassium permanganate, 10 mL of hydrogen peroxide was added. The solution was centrifuged at 15000 rpm for 1 hour at 4°C to separate the residues. The residues were then dispersed in ethanol, and the floating fluid on the surface was collected. Centrifugation at 5000 rpm for 1 hour at 4°C was carried out to remove unreacted CNTs. The unreacted or non-exfoliated carbon nanotubes are usually collected in the upper layer of the liquid (supernatant) after centrifugation.[47]



Schematic1.Synthesis mechanism of DF-GNR

For the preparation of DF-GNR, in a reflux condenser-equipped two-neck round bottom flask with a capacity of 50 mL, GONR (0.5 g) and BMIBr (2 g) were added. Then, triphenyl phosphate (0.5 mL) was introduced to the mixture of reaction, and finally, doxorubicin (1 g) was added and stirred for 20 min. For 2 hours, the mixture was heated to 100°C. Subsequently, the final product was washed with methanol, filtrated, and dried for 10 hours at 80°C in an oven [48].

The reaction mechanism between triphenyl phosphate, BMIBr and the formation of DF-GNR is described in the supporting information file. [48]

2.4. Standard and nanocomposite electrolytes preparation

Instead of employing organic solvents, the same concentration of 1 M of both EMII and BMII ILs was utilized to create the electrolytes. The standard electrolyte was created using 0.1 M LiI, 0.5 M TBP, and 0.1 M I₂ in a mixture of ILs. The standard electrolyte was combined with the various concentrations of DF-GNR (0.25, 0.5, 0.75, and 1 wt %) to create the nanocomposite electrolytes. After 30 minutes of sonication, the nanocomposite electrolytes were deposited on a stirrer with magnets for 24 hours to equally distribution of the DF-GNR in the ILs. It was thoroughly investigated that how the new nanocomposite-electrolytes affected the DSSCs' characteristics and performance.

2.5. Fabrication of DSSCs

The method for fabricating a solar cell employed in this project is the same as described in the publications.[21,45] Glass substrates with fluorine-doped tin oxide (FTO) are washed. Then, based on the Dr. Blade method, a coating of TiO₂ with a particle size of about 25 nanometers is printed on the conductive surface of some portions, followed by a layer of scattering paste with a particle size of about 400 nanometers. They are heated to 500 degrees Celsius during a routine temperature program for this section. Finally, a translucent film with an area of 0.16 square centimeters and a thickness of 8 micrometers is obtained. These components are immersed in a solution of dye (N719) at room temperature for 18 to 24 hours to allow the nano-crystalline fraction to absorb the dye. To prepare the cathode, a 0.6 mm diameter micro mill is used to make holes for electrolyte injection, and then the pieces are washed in the same way as the anode. Then, on the entire glass surface, a solution of H₂PtCl₆ in absolute ethanol is evenly deposited. The glasses are heated to a temperature of around 460°C for about 15 minutes and then cooled slowly. Through a previously-made hole on the cathode, the electrolyte enters the empty area between the two electrodes and creates a vacuum. A piece of serlin is inserted in the hole to prevent the electrolyte from leaking out, and a piece of hot glass is placed on the serlin to adhere to it thoroughly. The electrochemical study of the completed solar cell is now possible.

Two types of electrolytes, standard and nanocomposite, were employed to create cells in this project, with interesting results.

2.6. DFT Method

To examine the impact of incorporating DF-GNR into electrolytes as an effective additive to improve the efficiency of DSSCs, calculations of density functional theory (DFT) [49,50] were conducted. These calculations focused on investigating the electronic properties of the interfaces in DSSCs. The Vienna ab initio simulation package (VASP) was used in the geometry optimization procedure[51,52], utilizing the generalized gradient approximation (GGA) and a plane-wave basis set[53] implemented through the method named projected-augmented wave (PAW)[54] and the Perdew-Burke-Ernzerhof (PBE) functional.[55].

The PBE0 hybrid functional was used to calculate the electrical characteristics and get precise band gap values[56–58]. Additionally, the dispersion correction based on the Grimme Scheme [59] was applied. Based on the Monkhorst Pack scheme, A cutoff energy of 500 eV and a Γ point grid were used for the growth of the plane wave basis sets and the Brillouin zone sampling, respectively[60]. The geometry optimization process continued until a convergence criterion of 0.01 eV/Å for the maximum force on atoms and 10⁻⁵ eV for energy was achieved.

2.6.1. DFT Model

In our research, we selected the anatase TiO₂ (101) facets as the electrode due to their stable nature.[61–63] To better comprehend the electrical structures near the interface between the electrolyte and the TiO₂ (101) electrode employed in our project, we constructed and improved adsorbed structures of doxorubicin-functionalized GNR (graphene nanoribbon) containing ILs (ionic liquids) and TBPs (tert-butylpyridine) as the primary components of the standard electrolyte on the surface of TiO₂ (101). This configuration is illustrated in Figure 1.

The calculated lattice constants of a and b were found to be 3.784 Å, and c was determined to be 9.514 Å, which closely align with experimental values for bulk TiO₂ anatase.[64] Our model of the anatase TiO₂ (101) surface consisted of four fixed layers at the bottom and four relaxed layers on top, in accordance with existing literature.[65]

To model the electrolyte system, we first optimized the structures of IL, TBP, and doxorubicin, as shown in Figures 1.a to 10.c. Following this, IL and TBP molecules were incorporated onto the TiO₂ surface (Figure 1.d) as vital components of the standard electrolyte to evaluate their roles in enhancing ion transport and supporting electron transfer at the interface. Next, a GONR layer with randomly placed carboxyl and hydroxyl functional groups on its edges was constructed. Doxorubicin was then used to functionalize the GNR, creating DF-GNR, onto which ILs and

TBPs were subsequently introduced. The interactions between these components and the TiO₂ surface were analysed, as depicted in Figure 1.e. This comprehensive configuration enabled the study of mid-gap states' formation and their influence on the electronic properties of the system, contributing to improved DSSC performance.

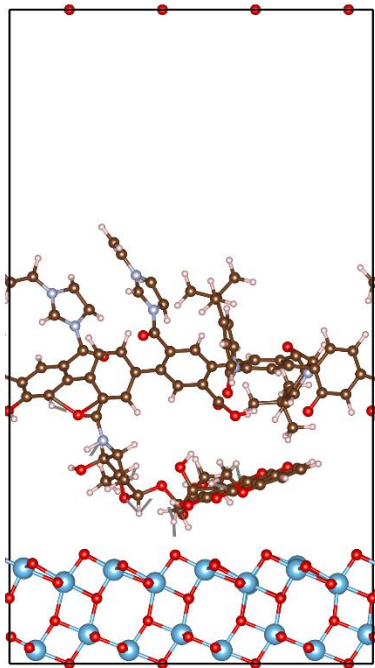


Fig. 1. The lowest energy structures of a) TBP, b) IL and c) Doxorubicin, d) IL/TBP/TiO₂, and e) IL/TBP/DF-GNR/TiO₂; Brown spheres stand in for carbon atoms, red spheres for oxygen atoms, larger blue spheres for titanium atoms, smaller blue spheres for nitrogen atoms, and white spheres for hydrogen atoms.

3. Results and discussion

3.1. Characterization of GONR and DF-GNR

The FTIR spectra (by FTIR spectrometer made in U.S.A, PerkinElmer Spectrum1 model) of DF-GNR and GONR are shown in Fig. 2. The GONR spectrum exhibits some common peaks at 3400, 1725, 1285, and 1069cm⁻¹, that are credited to O-H stretching, C=O stretching, C-OH stretching, and C-O vibrations, respectively.[66–70] In addition, GONR peaks are compatible with fingerprint bonds such as C=O vibrations (1625 cm⁻¹), and O-H bending (662 cm⁻¹)[67,71]. It also displays the distinctive peak at 2927 cm⁻¹ that is connected to the C-H stretching vibrations.[72] In the DF-GNR spectrum, the sharp band at 1719 cm⁻¹ belongs to the carbonyl group in doxorubicin. Another intense peak at 1034 cm⁻¹ represented the C-O stretching bond. Also, the graph shows a peak at 3396 cm⁻¹ relating to the vibration of the O-H bond and a band around 1583 cm⁻¹ connected to the aromatic rings in doxorubicin.[73] In addition, the N-H tensile band of 3168 cm⁻¹ is related to the structure of doxorubicin which indicates the successful

functionalizing process [74], and the peak of 2970 cm^{-1} represents the symmetric vibrations of NH_3^+ that is no longer visible in the DF-GNR spectrum due to the amide bonds formation. This investigation revealed particular peaks at wave numbers 682, 813, 1140, 1402 and 1644 cm^{-1} that correspond to C=C ring bending, C-H bending, aromatic C-H, carboxylic acids, alkenyl C=C stretch, respectively.[75–82] In general, the results acquired from this analysis confirm the correct functionalization process of GONR.

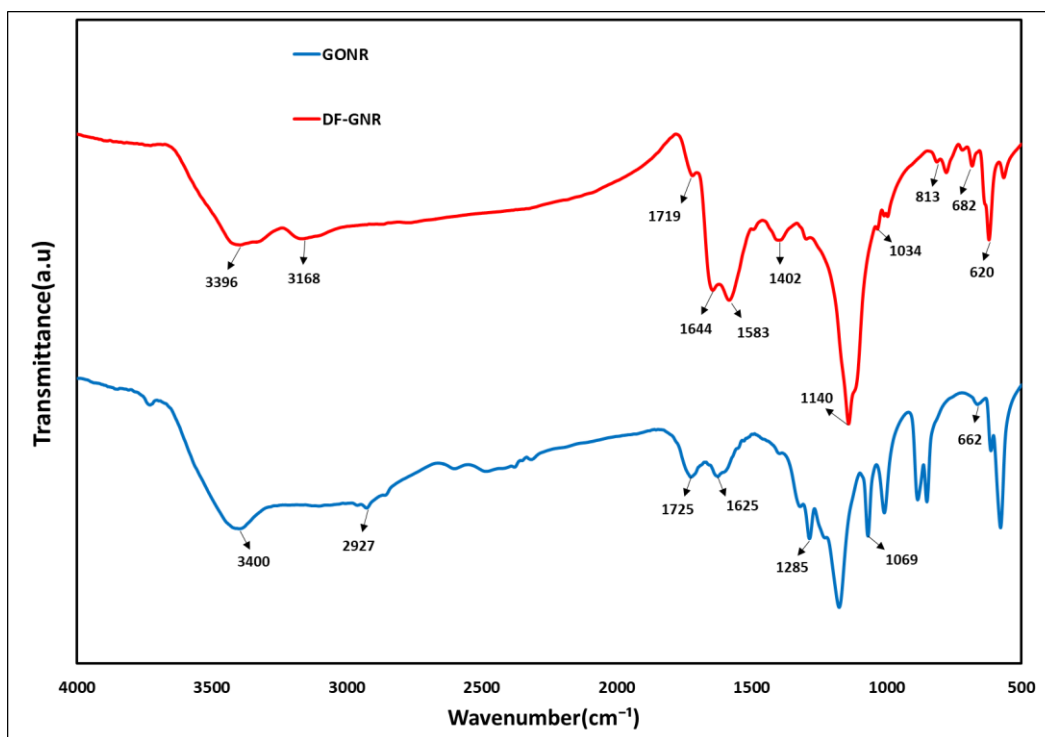


Fig. 2. The FT-IR of GONR and DF-GNR

The XRD pattern (XRD spectrometer made in Netherlands, Philips pw1730 model) that is depicted in Fig. 3 shows a very clear peak with high intensity at 32.12° and a d-spacing of 2.74 nm for the DF-GNR, which characterizes the structure of doxorubicin. In the diffraction pattern of Dox in its crystalline and purest state, this peak is formed at 31.24° . The increase in this angle and its high intensity are evidence of the presence of a large amount of it in the synthesized material and the reduction of GONR. Other characteristic peaks of doxorubicin are 25.42° and 38.94° with d-spacing of 3.46 and 2.22 nm, respectively. Comparing the peaks in GONR and DF-GNR, it can be seen that after the oxidized nanoribbon is modified, the d-spacing and angle increase. This is because there is a lot of oxygen in the GONR structure, which is reduced.[66,71,83]

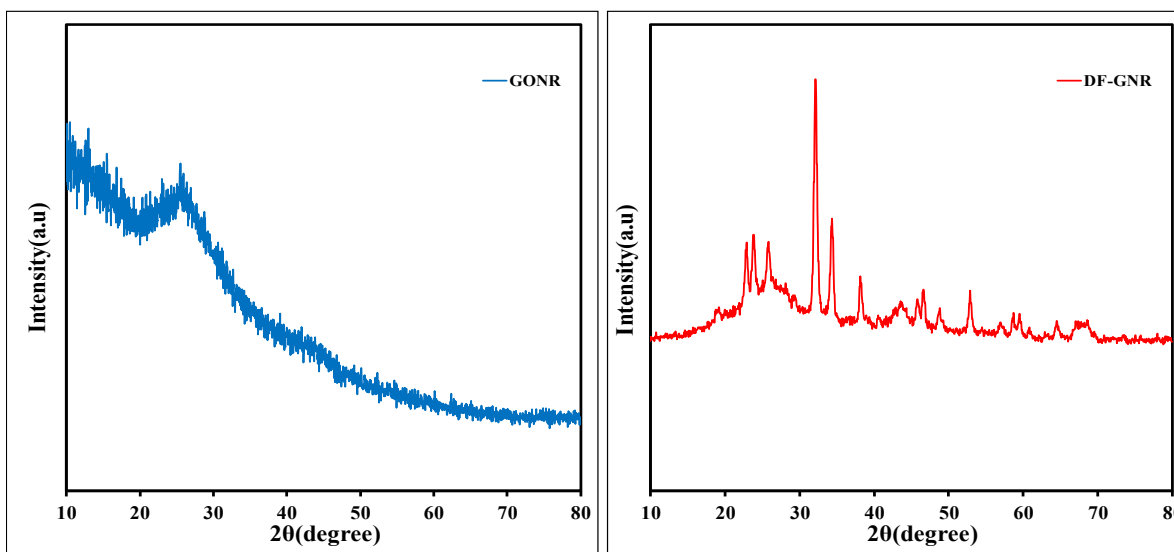


Fig. 3. XRD patterns of GONR and DF-GNR

In the Raman spectrum (Raman spectrometer made in Iran by Teksan company, TakRam N1-541 model) of GONR shown in Fig. 4, two high-intensity peaks of about $\sim 1580\text{cm}^{-1}$ (G band) corresponded to the carbon sp^2 internal vibration and $\sim 1330\text{cm}^{-1}$ (D band) corresponded to changes in the graphene edges and vibration of C atoms' stretching in sp^3 can be observed[84]. The mentioned peaks are also visible in DF-GNR spectrum with different intensities. An increase of I_D/I_G values in the calculation for DF-GNR compared with GONR can be seen, which can be attributed to the formation of amide bonds between doxorubicin and GONR. There is a peak at 1290cm^{-1} which is a sign of hydrogen bonds in doxorubicin. The carboxylic acid groups in the structure also peaked at 1625cm^{-1} and 1687cm^{-1} . In the $700\text{-}750\text{ cm}^{-1}$ range, the amide group in the DF-GNR has a very weak peak. Furthermore, the peaks in the region $2675\text{-}2940\text{cm}^{-1}$ in DF-GNR spectra belong to the CH-X groups, which is intense due to the addition of doxorubicin to the structure. In general, the characteristic peaks of GONR are more intense in the DF-GNR spectrum, which can be attributed to the relative reduction of GONR and the formation of a bond with doxorubicin. One of the factors affecting the intensity of Raman peaks is the vibration of electron pairs, which depends on the π bonds in the structure.[76,85–88]

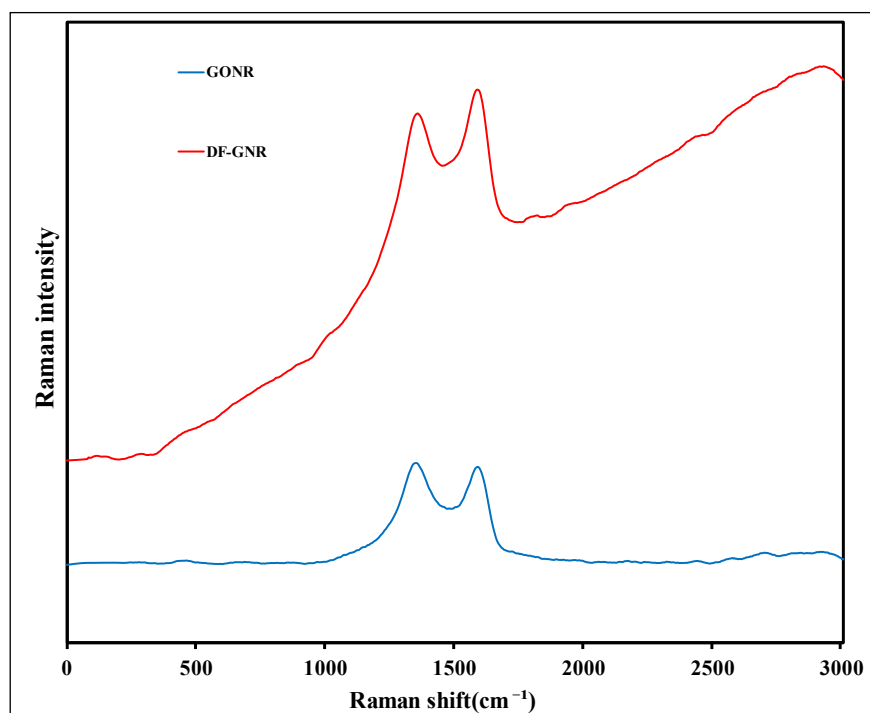


Fig. 4. Raman spectra corresponding to GONR and DF-GNR

X-ray photoelectron spectroscopy (XPS) is a valuable measurement method to determine the elemental chemical compounds across the surface of materials.[17] According to Fig. 5, the presence of C 1s, O 1s, and N 1s peaks verifies the existence of carbon, oxygen, and nitrogen elements in the graphene nanoribbon sample functionalized by doxorubicin. Employing CasaXPS software, the spectra were analyzed to calculate atomic percentages of oxygen, carbon, and nitrogen elements of 11.37%, 85.04%, and 3.60%, respectively. Table 1 displays the atomic percentage analysis using the survey spectrum, whereas Fig. 5 displays the deconvolution of high-resolution XPS spectra of the C 1s, O 1s, and N 1s elements in the DF-GNR.

Table 1. Analysis of the atomic percentages of the DF-GNR survey spectrum using XPS

Peak	Assignments	Binding energy (eV)	Fitted peak area (CPS.eV)	Atomic percentage (%)
	C=O	530.20	660.5	4.35
O 1s	C-O	532.15	13577.9	89.50
	O-C=O	535.35	932.8	6.15

C 1s	C-C/C=C	284.30	10207.6	30.55
	C-N	284.71	6963.7	20.84
	C-OH	285.13	1111.8	3.33
	C-O-C	285.95	10590.7	31.70
	C=O	287.91	4534.3	13.57
N 1s	N-H	399.25	495.5	19.11
	C-N	400.35	2096.9	80.89

The deconvoluted O 1s peaks with binding energies of 530.20, 532.15, and 535.35 eV referring to C=O, C-O, and O-C=O bonds, respectively, in the DF-GNR structure (based on Table 1 and Fig. 6). Also, the C 1s peak is separated into five distinct peaks at 284.30, 284.71, 285.13, 285.95, and 287.91 eV related to C-C and C=C bonds in aromatic rings, C-N bonds in doxorubicin, C-OH, C-O-C and C=O bonds, respectively[89]. In addition, the N 1s is divided into two peaks at 399.25, and 400.35 eV, which are related to N-H and C-N bonds in doxorubicin[90].

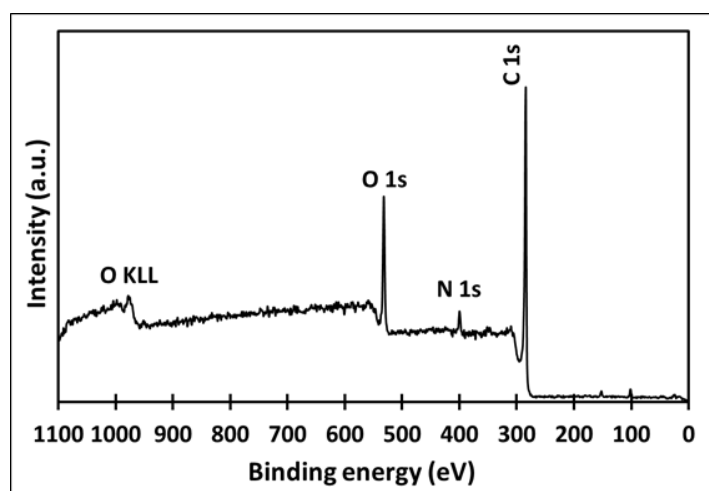


Fig.5. XPS survey spectrum of the DF-GNR

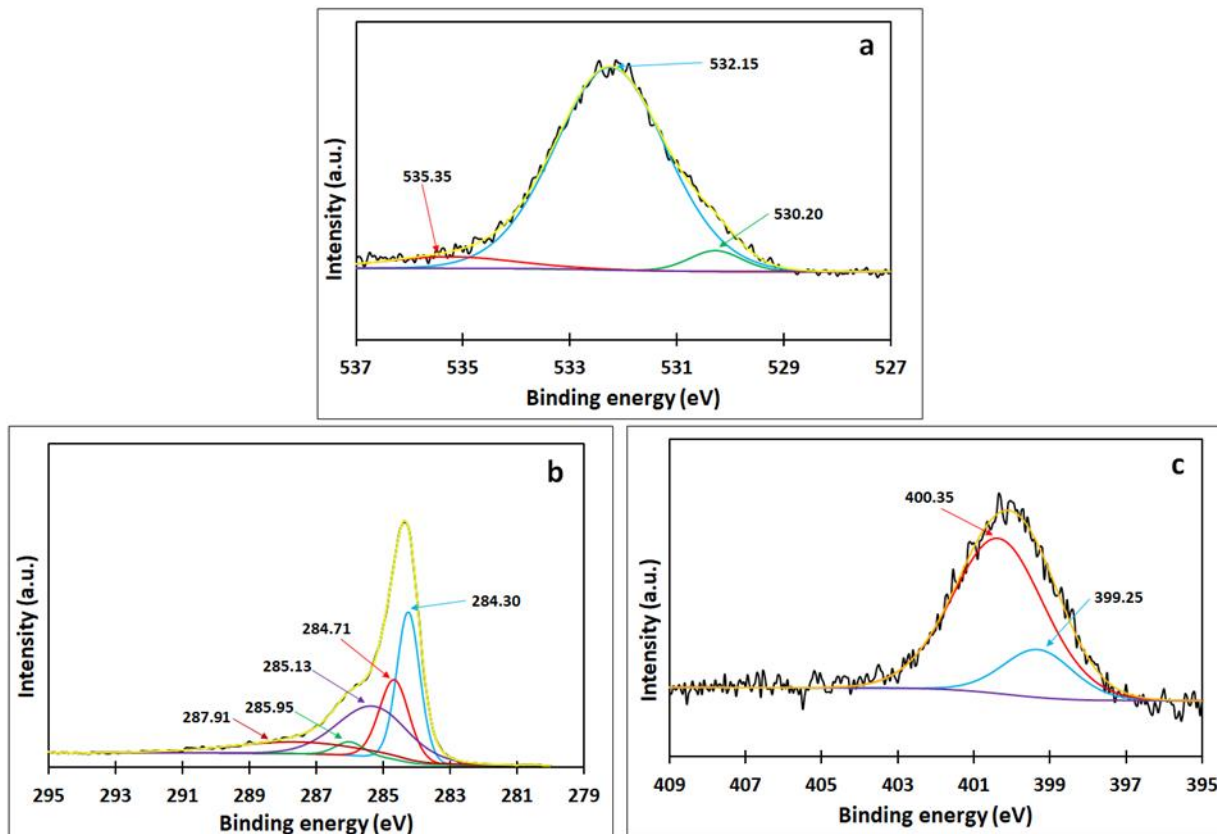


Fig.6.peak-fitting XPS spectrum of (a) O1s, (b) C1s, and (c) N1s of DF-GNR with High-resolution

Fig. 7 illustrates the TEM images of DF-GNR recorded at various magnifications (TEM instrument made in Netherlands, philips EM208s model). At higher magnifications, the three-dimensional graphene structures in the form of ribbons and intertwined strands (Fig7.a) can be seen. In some images, opened carbon nanotubes with empty spaces (Fig7.b) are visible. The darker areas in the images are probably related to the accumulation of dense masses due to the bonding of the doxorubicin structure to the GONR edges and the synthesis of amide. [91,92] Such a bonding mechanism just specifies the particular chemical interaction in this paper that occurred between carboxylic groups situated on the edges of GONR with the amine groups from doxorubicin through covalent bonding by the amide bond confirmed through XPS and FTIR spectra. [22]

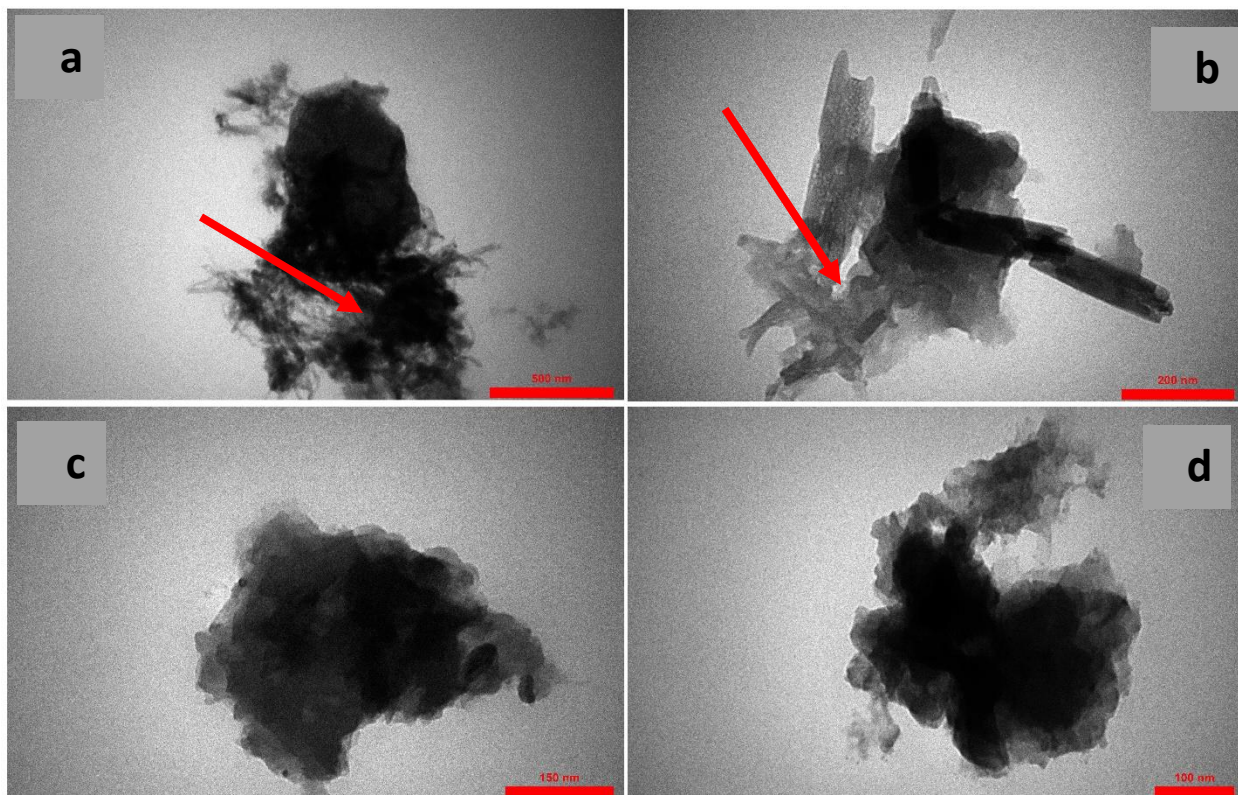


Fig. 7. TEM images of DF-GNR

Fig. 8 presents the FESEM images of DF-GNR (FESEM instrument made in U.S.A, Quantum 200 model). In the images after GONR is functionalized and modified by Dox, it can be seen that the graphene plates have become highly integrated and dense due to the amide bond formation at the edges and have been reduced to smaller particles. Nevertheless, wrinkles are still seen on the edges (Fig 8.a) , which is a prominent feature of graphene (high surface area).[67,93,94]

While most interesting, this interaction and successful functionalization between GONR and doxorubicin are elaborated through the results in FTIR, Raman, and XPS spectroscopy carried out for DF-GNR. Besides, the deconvoluted peak fitted with the oxygen-containing group and amide bonds at C=O 530.20 eV, N-H, and CN of 399.25 eV and 400.35 eV also agree with the process of chemical bonding in the XPS data. Complementary FTIR was done through the removal of NH_3^+ peaks and an increase in C=O and N-H stretching vibrations at 1719 cm^{-1} and 3168 cm^{-1} , respectively, due to the covalent attachment of doxorubicin. This is further supported from the Raman spectra, where an increased ID/IG ratio points toward structural alteration and thereby effective functionalization. These

findings verify that the binding of doxorubicin onto GONR is mainly due to chemical bonding from the amidation reaction, although minor contributions arise from physical interactions such as π - π stacking.[95,96]

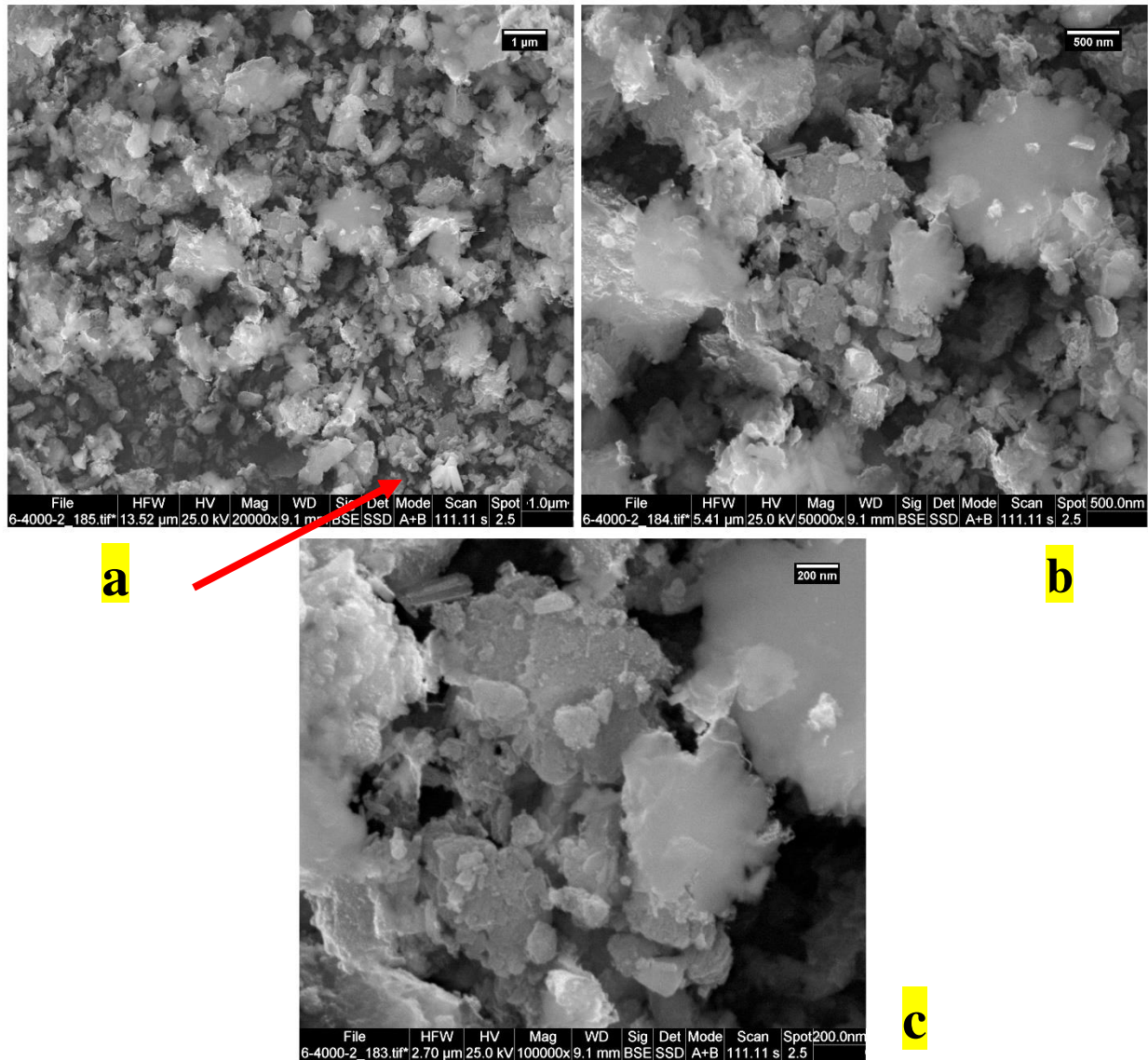


Fig. 8. FESEM images of DF-GNR

3.2. Photovoltaic performances of DSSCs

Four solar cells were built for each of five different types of electrolytes containing 0, 0.25, 0.5, 0.75, and 1 wt% of functionalized graphene nanoribbon. The electrolyte containing 0% DF-GNR by weight was evaluated as the standard electrolyte. Current-voltage analysis (I-V) was performed on these cells after they were placed in the simulator. Fig. 9 depicts the curves derived from this analysis for several cell types based on the electrolyte utilized. In this section,

the derived (I-V) curves subjected to intense light are studied and evaluated using a solar light simulator (Sharif Solar, SIM-1000) with an intensity (1000 Wm^{-2}) equivalent to AM 1.5 solar spectrum irradiation. In order to examine the electrolytes with varied DF-GNR percentages, the experiment was performed in four identical cells containing the same type of electrolyte, and the average data is given in Table 2.

Adding DF-GNR to the electrolyte increases the efficiency (μ), open-circuit voltage (V_{OC}), and current density (J_{SC}) in general; however, the rise differs depending on the graphene weight percentage employed. Adding 0.5% by weight of DF-GNR to the electrolyte produces the optimum current density (J_{SC}) and efficiency (μ) among all the cells. Consequently, 0.5% by weight is the ideal concentration for this type of DF-GNR. By adding the functionalized substance to the electrolyte at a rate of 0.25 and 0.5 wt% due to the special GNR's structure, the presence of heterocyclic structure, and the free electron pairs in doxorubicin, the electron transfer increased, and as a result, the redox reaction became faster. This has enhanced the current density (J_{SC}) and efficiency (μ), and due to decreasing the rate of charge recombination process, open-circuit voltage (V_{OC}) has grown. However, with adding 0.75 to 1 wt%, due to the rise in the quantity of molecules of the additive in the electrolyte, the viscosity of the electrolyte rose, and electron transfer became difficult. Therefore, the electron resistance has grown, and the current and efficiency have dropped.

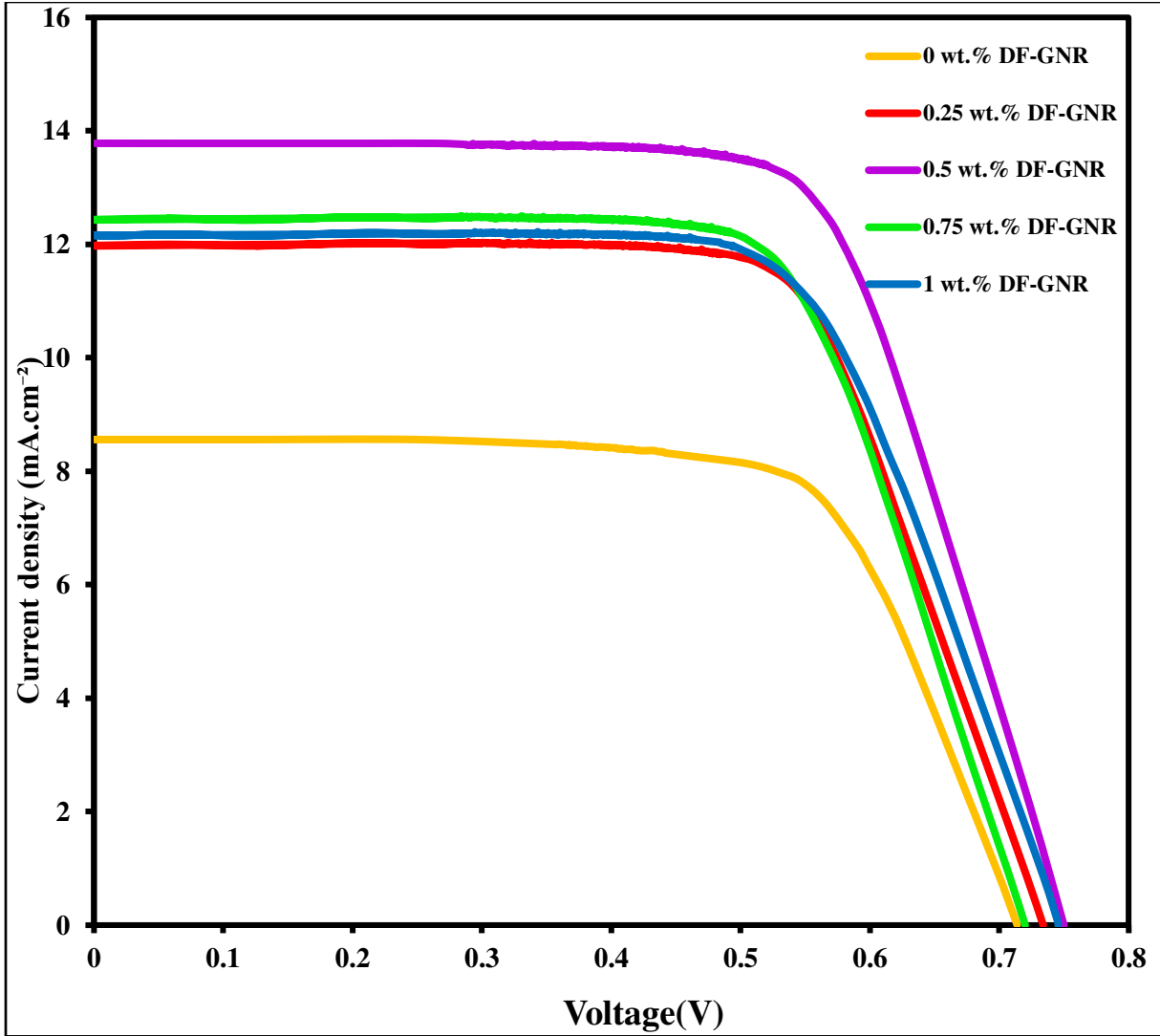


Fig. 9. Current density-voltage (J-V) curve of DSSCs employing various DF-GNR concentrations in the electrolytes

Table 2. Photovoltaic characteristics derived from DSSCs' J-V curves utilizing the standard electrolyte and various concentrations of DF-GNR in electrolytes

Cells	η [%]	FF	J_{sc} [mA/cm ²]	V_{oc} [V]
E₀ (0 wt.% DF-GNR)	4.276	0.699	8.559	0.713
E₁ (0.25 wt.% DF-GNR)	6.089	0.688	12.042	0.733
E₂ (0.5 wt.% DF-GNR)	7.126	0.689	13.781	0.749
E₃ (0.75 wt.% DF-GNR)	6.178	0.686	12.502	0.720
E₄ (1 wt.% DF-GNR)	6.118	0.671	12.222	0.745

3.3. Electrochemical performances of DSSCs

In order to do electrochemical impedance spectroscopy (EIS) by IviumStat.XRe, the solar cell is subjected to a constant potential bias and a slight sinusoidal potential disturbance. This minor perturbation in the potential induces a sinusoidal disruption in the current. Obtaining the equivalent circuit permits the calculation of the system's electron transport parameters. EIS analyzes the resistors in solar cells that have been manufactured. The final outcome of this spectroscopy is depicted in the Nyquist diagram in Fig. 10. The best approximation of the number of circuit parameters equal to the DSSCs is generated by the ZView software. This analysis is measured for two types of solar cells created with standard electrolyte and nanocomposite electrolyte with the appropriate amount of DF-GNR (0.5wt %) under 20 mV AC sunlight simulator radiations in the range of frequency reaching 0.01 to 100 kHz. Table 3 defines the resistor types, such as the counter electrode resistance (R_1), the titanium dioxide-electrolyte-dye resistor (R_2), the Warburg resistor related to the oxidation / electrolyte coupling penetration process (R_{Diff}). Series resistors consist of TCO layer resistors and junction resistors (R_s). By adding the optimal amount of DF-GNR to the electrolyte, it is possible to conclude that all real resistors are lowered, and as a result, cell performance is enhanced with the DF-GNR composite electrolyte.[97] The results are shown in Table 3. It can be said that in general, the unique 3D structure of graphene nanoribbon and doxorubicin and the new amide bond established between them have caused more electrons to flow and facilitate redox reactions in the electrolyte. Therefore, increasing the electron transfer by adding an additive to the electrolyte leads to a drop in the electron resistance (R) compared to the standard electrolyte.

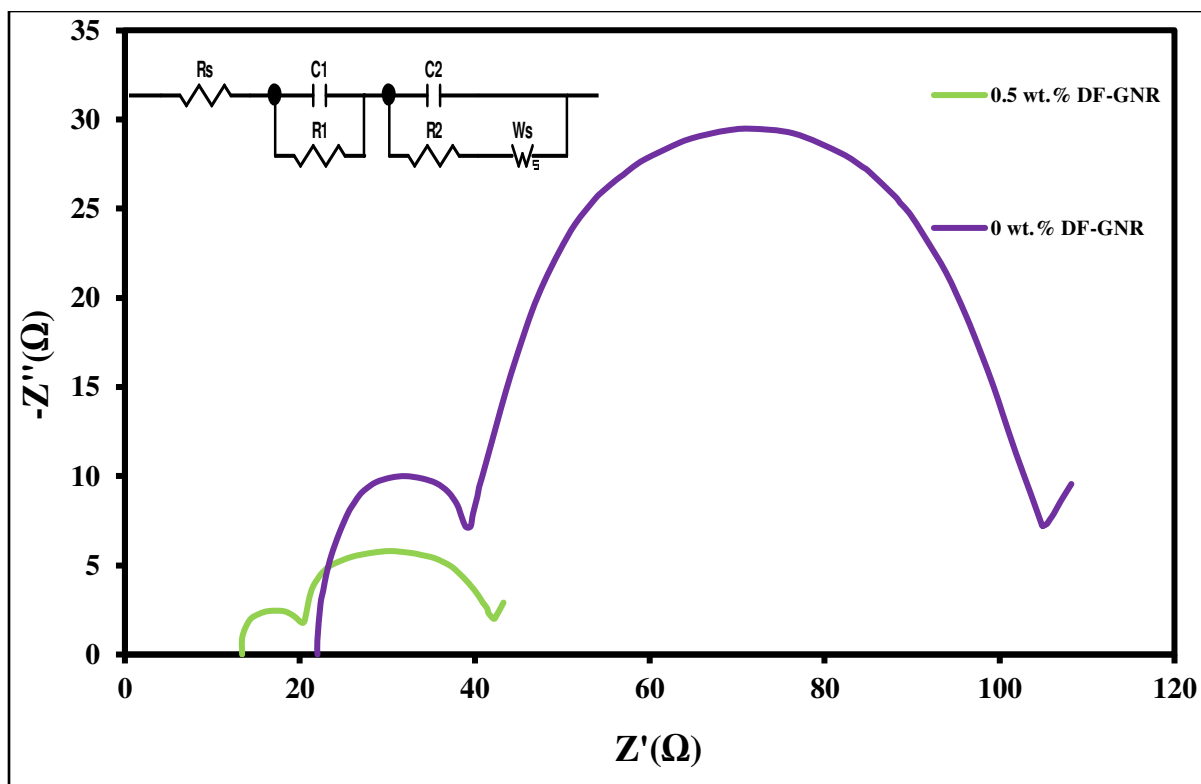


Fig. 10. The DSSCs' EIS spectrum with the standard (E0) and nanocomposite electrolyte (E2)

Table 3. Parameters of EIS calculated by utilizing ZView software to fit the experimental data

Cells	$R_s(\Omega)$	$R_1(\Omega)$	$R_2(\Omega)$	$R_{diff}(\Omega)$
E₀ (0 wt. % DF-GNR, standard electrolyte)	22.015	17.197	65.748	73.652
E₂ (0.5 wt. % DF-GNR, nanocomposite electrolyte)	13.400	6.958	21.830	28.231

3.4. Computational calculations (DFT Results)

This study aimed to investigate the electronic properties of a nanocomposite system comprising the adsorption configuration of the examined electrolyte on the surface of anatase TiO_2 (101). The goal was to acquire improved knowledge about the impact of the new electrolyte additive on the TiO_2 electrode-electrolyte interactions.

Figure 11 illustrates the total and projected states' density for the investigated nanocomposite. The results reveal the presence of midgap states within the bandgap of TiO_2 attributed to the incorporation of DF-GNR in the electrolyte. Mid-gap states are electronic states that form within the energy gap of a semiconductor due to defects, impurities, or

the incorporation of foreign materials like DF-GNR. These states can act as pathways for electron transport, enhancing conductivity and facilitating charge transfer in the system. These mid-gap states, introduced by DF-GNR and influenced by the surrounding ILs and TBPs, are absent in pristine TiO_2 and provide pathways for enhanced electronic conduction. It is important to note that the initial band gap of anatase TiO_2 without additives was 3.2 eV, which was reduced due to the introduction of mid-gap states when DF-GNR, ILs and TBPs were incorporated. Consequently, this outcome causes a redshift in the adsorption edge and leads to an enhancement in the efficiency of DSSCs. These results provide more evidence that DF-GNR, a novel addition to the conventional electrolyte, increases composite conductivity and speeds up electron transmission across the interface between TiO_2 and the electrolyte.

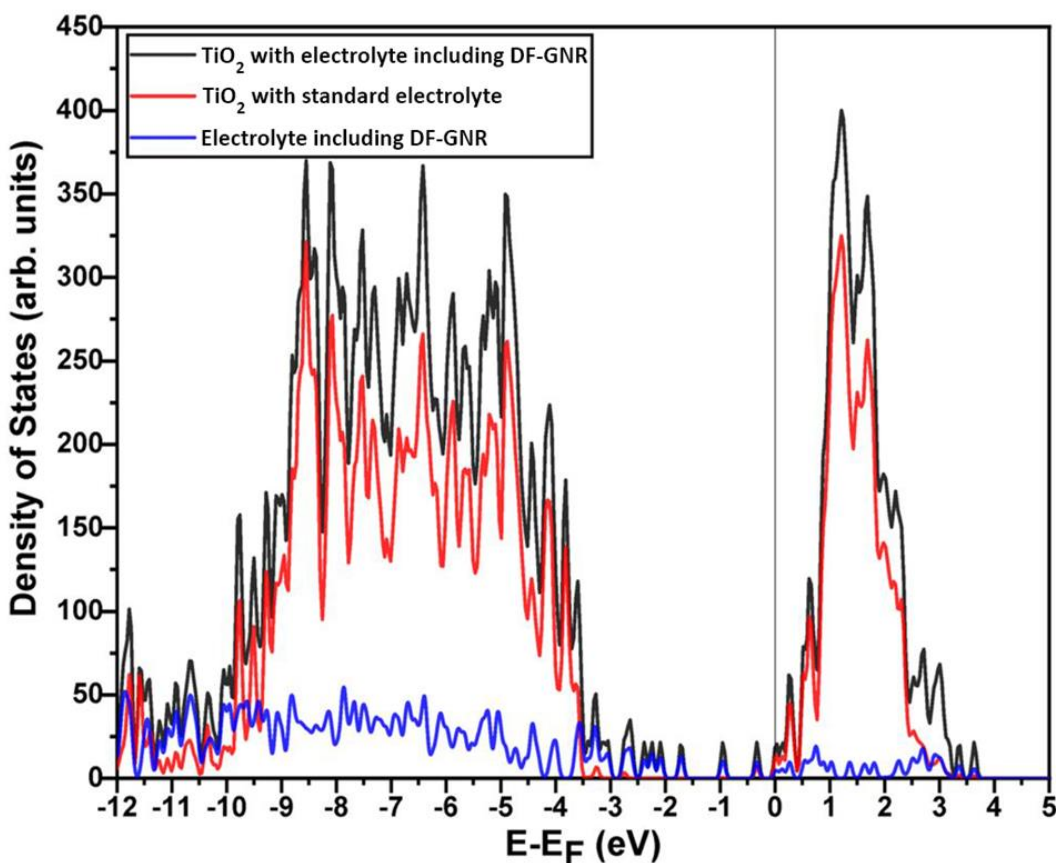


Fig. 11. The computed density of states (DOS) for the adsorption configuration of the doxorubicin-functionalized graphene nanoribbon (DF-GNR) incorporating ILs and TBPs as the standard electrolyte on the anatase TiO_2 (101) surface. The energy distribution of electronic states in the system is shown by the computed DOS, where the Fermi level is located at 0 eV.

4. Conclusions

A novel and effective additive of DF-GNR was synthesized and utilized in DSSCs containing BMII and EMII ILs-based electrolyte so as to enhance their performance. This supplement caused remarkable electrochemical results. By

applying the optimal amount of 0.5wt% DF-GNR in the nanocomposite electrolyte under AM 1.5 simulated solar light illumination, the conversion efficiency of DSSC was increased to 7.126% from 4.276% (with the standard electrolyte). The incredible 3D structure of the ribbons, along with the significant effect of doxorubicin contributed to this higher efficiency. To be more precise, GNR's exceptional electronic properties, high surface area, and π electrons made it electrochemically special. Also, Doxorubicin was employed to chemically modify GONR through the Vilsmeier reaction and create an amide bond in the final compound. This bond and the structure of GNRs quickened the charge transfer by hastening the redox pair (I^-/I_3^-) reaction inside the electrolyte. Moreover, doxorubicin includes aromatic rings, oxygen, and nitrogen groups, which increase the number of free electron pairs and the final composition's conductivity. The DFT calculations demonstrated that the addition of DF-GNR as a new additive to the standard electrolyte resulted in the emergence of midgap states within the bandgap of TiO_2 . This phenomenon led to an increase in composite conductivity and facilitated electron transfer. Therefore, it boosted the effectiveness of GNR in relation to improving the performance of DSSCs.

Credit authorship contribution statement

M. D.: Writing – original draft, Data curation, Formal analysis, Methodology, Writing – review & editing, Investigation. **E.K:** Conceptualization, Methodology, Supervision, Editing, Project administration, Funding acquisition, Writing – review & editing, Investigation, Formal analysis. **M M B:** Methodology, Formal analysis, Visualization, Writing – review & editing. **S. S.T:** Formal analysis, Data curation, Writing – review & editing. **M. R. C.:** Formal analysis, Data curation, Writing – review & editing. **N. H. d. I.:** Methodology, Formal analysis, Writing – review & editing. All authors reviewed the manuscript."

Funding. The authors acknowledge the financial support supplied by the Research Affairs Division of Amirkabir University of Technology (AUT) in Tehran, Iran. This research utilized the ARCHER2 UK National Supercomputing Service (<http://archer2.ac.uk>) through our membership in the EPSRC (EP/R029431)-funded HEC Materials Chemistry Consortium in the United Kingdom. The computational resources of the Advanced Research Computing at Cardiff (ARCCA) Division, Cardiff University, and HPC Wales were employed as well for this study.

Acknowledgment

The authors express their deepest gratitude to Professor Seeram Ramakrishna of the National University of Singapore for his invaluable help, insights, and unwavering guidance throughout the development of this article.

Availability of Data and Materials Not applicable

Declarations

Conflict of interest/ Competing Interests Prof. Elaheh Kowsari is a member of the editorial board for Research on Chemical Intermediates. All other authors declare no competing interests.

Ethical approval Not applicable.

References

- [1] S. Orangi, E. Kowsari, M. Mohammadizadeh Boghrabad et al., *J. Mol. Liq.* **397**, 124057 (2024)
- [2] W.J. Wu, W.H. Zhan, J.L. Hua, H. Tian, *Res. Chem. Intermed.* **34**, 241 (2008)
- [3] T. Toyao, M. Minakata, K. Iyatani et al., *Res. Chem. Intermed.* **39**, 415 (2013)
- [4] W. Liu, Z. Feng, W. Cao, *Res. Chem. Intermed.* **39**, 1623 (2013)
- [5] J. Hu, X. Jin, D. Peng et al., *Res. Chem. Intermed.* **41**, 8327 (2015)
- [6] L. Han, J. He, J. Zhao, S. Jiang, *Res. Chem. Intermed.* **43**, 5779 (2017)
- [7] H. Sadki, M. Bourass, M.N. Bennani, M. Bouachrine, *Res. Chem. Intermed.* **44**, 6071 (2018)
- [8] O. Wiranwetchayan, W. Promnopas, K. Hongstith et al., *Res. Chem. Intermed.* **42**, 3655 (2016)
- [9] H. Liu, Y. Lou, S. Yuan et al., *Res. Chem. Intermed.* **43**, 4881 (2017)
- [10] M. Lazrak, H. Toufik, S.M. Bouzzine, F. Lamchouri, *Res. Chem. Intermed.* **46**, 3961 (2020)
- [11] S. Cogal, S. Erten Ela, A.K. Ali et al., *Res. Chem. Intermed.* **44**, 3325 (2018)
- [12] O. Wiranwetchayan, W. Promnopas, S. Choopun et al., *Res. Chem. Intermed.* **43**, 4339 (2017)
- [13] R. Kacimi, M. Bourass, T. Toupance et al., *Res. Chem. Intermed.* **46**, 3247 (2020)
- [14] X. Wang, Q. Sun, L. Qi, *Res. Chem. Intermed.* **46**, 1705 (2020)
- [15] R. Sivakumar, S. Anandan, *J. Mol. Liq.* **172**, 8 (2012)
- [16] S. Ramkumar, K.-G. Upul Wijayantha, D. Velayutham, S. Anandan, *J. Mol. Liq.* **193**, 185 (2014)

- [17] M. Rafieepoor Chirani, E. Kowsari, S. Ramakrishna et al., *J. Mol. Liq.* **364**, 119999 (2022)
- [18] S.K. Tseng, R.H. Wang, J.L. Wu et al., *Polymer (Guildf)*. **210**, 123074 (2020)
- [19] P.T. Nguyen, T.D.T. Nguyen, V.S. Nguyen et al., *J. Mol. Liq.* **277**, 157 (2019)
- [20] S. Venkatesan, Y.-Y. Chen, H. Teng, Y.-L. Lee, *J. Alloys Compd.* **903**, 163959 (2022)
- [21] M.M. Boghrabad, E. Kowsari, S. Ramakrishna et al., *J. Alloys Compd.* **945**, 169241 (2023)
- [22] M.R. Chirani, E. Kowsari, H. SalarAmoli et al., *J. Mol. Liq.* **325**, 115198. (2021)
- [23] M.D. Najafi, E. Kowsari, H.R. Naderi et al., *Compos. Sci. Technol.* **211**, 108844 (2021)
- [24] M. Bigdeloo, E. Kowsari, A. Ehsani et al., *J. Energy Storage* **37**, 102474 (2021)
- [25] N. Neekzad, E. Kowsari, M.D. Najafi et al., *J. Mol. Liq.* **342**, 116962 (2021)
- [26] R. Aliakbari, E. Kowsari, H.R. Naderi et al., *J. Energy Storage* **50**, 104635 (2022)
- [27] F.B. Ajdari, E. Kowsari, H.R. Nadri et al, *Electrochim. Acta* **354**, 136663 (2020)
- [28] M. Dashti Najafi, E. Kowsari, H. Reza Naderi et al., *J. Mol. Liq.* **348**, 118381 (2022)
- [29] A.A. Ashtiani, E. Kowsari, V. Haddadi-Asl et al., *J. Mol. Liq.* **315**, 113697 (2020)
- [30] H. Ahmadi, V. Haddadi-Asl, E. Kowsari, N. Mohammadi, *J. Alloys Compd.* **927**, 167021 (2022)
- [31] S. Pandit, S. Seth (Duley), A. Bapli et al., *J. Mol. Liq.* **369**, 120880 (2023)
- [32] P. Mohammadzadeh Jahani, S. Tajik, H. Beitollahi et al., *Res. Chem. Intermed.* **45**, 5143 (2019)
- [33] H. Rezania, F. Azizi, *Solid State Commun.* **298**, 113638 (2019)
- [34] A.L. Higginbotham, D. V. Kosynkin, A. Sinitskii et al., *ACS Nano* **4**, 2059 (2010)
- [35] R. Nadiv, M. Shtein, M. Buzaglo et al., *Carbon N. Y.* **99**, 444 (2016)
- [36] F. Jabbari, A. Rajabpour, S. Saedodin, S. Wongwises, *J. Mol. Liq.* **282**, 197 (2019)
- [37] K. Nakada, M. Fujita, G. Dresselhaus, M.S. Dresselhaus, *Physical Rev. B* **54**, 954 (1996)
- [38] M. Fujita, K. Wakabayashi, K. Nakada, K. Kusakabe, *J. Phys. Soc. Japan* **65**, 1920 (1996)
- [39] Y.-W. Son, M.L. Cohen, S.G. Louie, *Phys. Rev. Lett.* **97**, 216803 (2006)
- [40] S. Venkatesan, E. Surya Darlim, *Carbon N. Y.*, **132**, 71 (2018)
- [41] W. Cheng, C. Wan, X. Li et al., *J. Energy Chem.* **83**, 549 (2023)
- [42] M. Negrette-Guzmán, *Eur. J. Pharmacol.* **859**, 172513 (2019)
- [43] A. Andooz, E. Kowsari, M.D. Najafi et al., *Electrochim. Acta* **477**, 143773 (2024)
- [44] D.G. Atinafu, J.Y. Choi, Y. Kang et al., *Trends Food Sci. Technol.* **147**, 104468 (2024)
- [45] E. Kowsari, M.R. Chirani, *Carbon N. Y.* **118**, 384 (2017)
- [46] T.-Y. Cho, S.-G. Yoon, S.S. Sekhon, C.-H. Han, *Bull. Korean Chem. Soc.* **32**, 2058 (2011)

- [47] K.M. Cho, S.Y. Cho, S. Chong et al., *ACS Appl. Mater. Interfaces* **10**, 42905 (2018)
- [48] S. Mallakpour, E. Kowsari, *J. Polym. Sci. Part A Polym. Chem.* **43**, 6545 (2005)
- [49] P. Hohenberg, W. Kohn, *Phys. Rev.* **136**, B864 (1964)
- [50] W. Kohn, L.J. Sham, *Phys. Rev.* **140**, A1133 (1965)
- [51] G. Kresse, J. Furthmüller, *Phys. Rev. B* **54**, 11169 (1996)
- [52] G. Kresse, J. Furthmüller, *Comput. Mater. Sci.* **6**, 15 (1996)
- [53] J.P. Perdew, K. Burke, M. Ernzerhof, *Phys. Rev. Lett.* **77**, 3865 (1996)
- [54] P.E. Blöchl, *Phys. Rev. B* **50**, 17953 (1994)
- [55] J. Paier, R. Hirschl, M. Marsman, G. Kresse, *J. Chem. Phys.* **122**, 234102 (2005)
- [56] J.P. Perdew, M. Ernzerhof, K. Burke, *J. Chem. Phys.* **105**, 9982 (1996)
- [57] M. Ernzerhof, G.E. Scuseria, *J. Chem. Phys.* **110**, 5029 (1999)
- [58] C. Adamo, V. Barone, *J. Chem. Phys.* **110**, 6158 (1999)
- [59] S. Grimme, S. Ehrlich, L. Goerigk, *J. Comput. Chem.* **32**, 1456 (2011)
- [60] H.J. Monkhorst, J.D. Pack, *Phys. Rev. B* **13**, 5188 (1976)
- [61] M. Lazzeri, A. Vittadini, A. Selloni, *Phys. Rev. B* **63**, 155409 (2001)
- [62] Y. Jiao, F. Zhang, M. Grätzel, S. Meng, *Adv. Funct. Mater.* **23**, 424 (2013)
- [63] H.G. Yang, C.H. Sun, S.Z. Qiao et al., *Nature* **453**, 638 (2008)
- [64] J.K. Burdett, T. Hughbanks, G.J. Miller et al., *J. Am. Chem. Soc.* **109**, 3639 (1987)
- [65] W. Orellana, *Sol. Energy* **216**, 266 (2021)
- [66] K.M. Cho, S.-Y. Cho, S. Chong et al., *ACS Appl. Mater. Interfaces* **10**, 42905 (2018)
- [67] P. Wu, Y. Wang, Y. Li et al., *J. Radioanal. Nucl. Chem.* **322**, 553 (2019)
- [68] A. Daghlavi, E. Kowsari, M. Abdouss et al., *Res. Chem. Intermed.* **46**, 3593 (2020)
- [69] M.B. Bakhshandeh, E. Kowsari, *Res. Chem. Intermed.* **46**, 2595 (2020)
- [70] H.D. Hanoon, E. Kowsari, M. Abdouss et al., *Res. Chem. Intermed.* **43**, 4023 (2017)
- [71] X. Hu, Y. Wang, J.O. Yang et al., *Chem. Sci. Eng.* **14**, 1029 (2020)
- [72] H.D. Hanoon, E. Kowsari, M. Abdouss et al., *Res. Chem. Intermed.* **43**, 1751 (2017)
- [73] H. Ahmed, A. Mokrish, R. Mansor et al., *J. Nanomedicine Volume* **14**, 3615 (2019)
- [74] A.A. Pozveh, E. Kowsari, M.M. Hashemi, Z. Mirjafari, *Res. Chem. Intermed.* **46**, 1329 (2020)
- [75] J.M. González-Domínguez, A. Colusso, L. Litti et al., *Chempluschem* **84**, 862 (2019)
- [76] F. Qiang, L. Hu, L. Gong et al., *Chem. Eng. J.* **334**, 2154 (2018)

- [77] Z. Hami, S.M. Rezayat, K. Gilani et al., *J. Pharm. Pharmacol.* **69**, 151 (2017)
- [78] G.J. Ilyas Khan, G. Joshi, K. T Nakhate et al., *Pharmaceutical Research*, **36**, 149 (2019)
- [79] R. Ganassina, C. Merker, M.C. Rodrigues et al., *Artificial Cells, Nanomedicine & Biotechnology*, **46**, 8 (2017)
- [80] S.P. Victor, W. Paul, M. Jayabalan, C.P. Sharma, *CrystEngComm* **16**, 9033 (2014)
- [81] R. Bansal, R. Singh, K. Kaur, *BMC Chem.* **15**, 1 (2021)
- [82] H. Takahashi, Junko and Iwahashi, *Clin Oncol.* **3**, 1330 (2017)
- [83] S. Mohanty, S. Sarangi, G.S. Roy, *Int. J. Appl. Pharm.* **11**, 138 (2019)
- [84] E. Kowsari, F. Morad, N. Seifvand et al., *Res. Chem. Intermed.* **46**, 1217 (2020)
- [85] J.H. Choe, J. Jeon, M.E. Lee et al., *Nanoscale* **10**, 2025 (2018)
- [86] C. Tapeinos, E.K. Efthimiadou, N. Boukos et al., *J. Mater. Chem. B* **1**, 194 (2013)
- [87] D Lin-Vien, NB Colthup, WG Fateley et al., in *Choice Rev.* **29** (1992)
- [88] C. Hirschl, L. Neumaier, W. Mühleisen et al., *Sol. Energy Mater. Sol. Cells* **152**, 10 (2016)
- [89] O. Akhavan, E. Ghaderi, H. Emamy, F. Akhavan, *Carbon N. Y.* **54**, 419 (2013)
- [90] S. Ravi, S. Zhang, Y.-R. Lee et al., *J. Ind. Eng. Chem.* **67**, 210 (2018)
- [91] Y. Wang, Z. Wang, Z. Gu et al., *J. Radioanal. Nucl. Chem.* **304**, 1329 (2015)
- [92] M. Wang, C. Wang, Y. Song et al., *Compos. Sci. Technol.* **165**, 124 (2018)
- [93] J. Al Dream, C. Zequine, K. Siam et al., *C* **5**, 18 (2019)
- [94] J. Kusuma, R.G. Balakrishna, S. Patil et al., *Sol. Energy Mater. Sol. Cells* **183**, 211 (2018)
- [95] M.H. Zainal-Abidin, M. Hayyan, G.C. Ngoh, W.F. Wong, *ACS Omega* **5**, 1656 (2020)
- [96] A.O.E. Abdelhalim, S. V. Ageev, A. V. Petrov et al., *J. Mol. Liq.* **359**, 119156 (2022)